

OPEN

3-D magnetohydrodynamic AA7072-AA7075/methanol hybrid nanofluid flow above an uneven thickness surface with slip effect

Iskander Tlili^{1,2}, Hossam A. Nabwey^{3,4}, G. P. Ashwinkumar^{5*} & N. Sandeep^{6*}

A 3-D magnetohydrodynamic flow of hybrid nanofluid across a stretched plane of non-uniform thickness with slip effects is studied. We pondered aluminum alloys of AA7072 and AA7072 + AA7075 in methanol liquid. The aluminum alloys amalgamated in this study are uniquely manufactured materials, possessing enhanced heat transfer features. AA7072 alloy is a composite mixture of Aluminum & Zinc in the ratio 98 & 1 respectively with added metals Silicon, ferrous and Copper. Equally, AA7075 is a mixture of Aluminum, Zinc, Magnesium, and Copper in the ratio of ~90, ~6, ~3 and ~1 respectively with added metals Silicon ferrous and Magnesium. Numerical solutions are attained using R-K based shooting scheme. Role of physical factors on the flow phenomenon are analyzed and reflected by plots and numerical interpretations. Results ascertain that heat transfer rate of the hybrid nanofluid is considerably large as matched by the nanofluid. The impact of Lorentz force is less on hybrid nanofluid when equated with nanofluid. Also, the wall thickness parameter tends to improve the Nusselt number of both the solutions.

Advanced electronic gadgets frequently encounter challenges because of heat control from enhanced thermal rise or reduction of available space for the thermal emission. Such drawbacks are overwhelmed by developing a preeminent model for heat-repelling gadgets or by amplifying thermal transport features. Nanofluid is a unique and well-suited fluid to fit for all needs. Initially, Choi¹ has experimented on the treatment of solid particles in conventional liquids to improve its thermal performance characterized as nanofluid. Due to its marvelous thermal and chemical properties, less volume and enhanced thermal properties, it is emerging as an extensively used cooling agent. Nanofluid has entered in many areas of science and engineering, and few are witnessed in nuclear cooling, biomedical applications, electronic cooling, etc. Because of its massive demand, it has attracted the research community to develop a new class of nanofluids. Few researchers⁽²⁻¹¹⁾ provided the theoretical and experimental studies for developing nanofluids in terms of preparation methods, applications and enhancing its thermal properties. Further, Animasaun *et al.*¹² deliberated the comparative study for distinct magnitude aluminum nanomaterials suspended in water, namely, 36 nanometers and 47 nanometers and predicted that 36 nm nanoparticle used to attain maximum flow velocity than other. Asadi *et al.*¹³ explained the flow of nanofluid (10 nanometer-sized Fe₃O₄ nanoparticles) across a sinusoidal crumpled section accounting the magnetic field effects. Later, Kumar *et al.*¹⁴ elaborated the stagnated flow caused by non-Newtonian liquids over a strained cylinder using C-C heat flux model. They concluded that friction factor parameter hikes significantly in Williamson liquid as compared with Casson liquid under the influence of thermal relaxation parameter. This kind of work was prolonged by Bai *et al.*¹⁵ using Oldroyd-B nanofluid.

MHD describes the magnetic properties of electrically conducting fluids. Theoretical investigation on CNT-water nanofluid motion through a rectangular region using Hamilton-Crosser model was scrutinized by

¹Department for Management of Science and Technology Development, Ton Duc Thang University, Ho Chi Minh City, Vietnam. ²Faculty of Applied Sciences, Ton Duc Thang University, Ho Chi Minh City, Vietnam. ³Department of Mathematics, College of Science and Humanities in Al-Kharj, Prince Sattam bin Abdulaziz University, Al-Kharj, 11942, Saudi Arabia. ⁴Department of Basic Engineering Science, Faculty of Engineering, Menoufia University, Shebin El-Kom, 32511, Egypt. ⁵Department of Mathematics, Vijayanagara Sri Krishnadevaraya University, Ballary, 583105, India. ⁶Department of Mathematics, Central University of Karnataka, Kalaburagi, 585 367, India. *email: ashwinpuje@gmail.com; nsandeep@cuk.ac.in

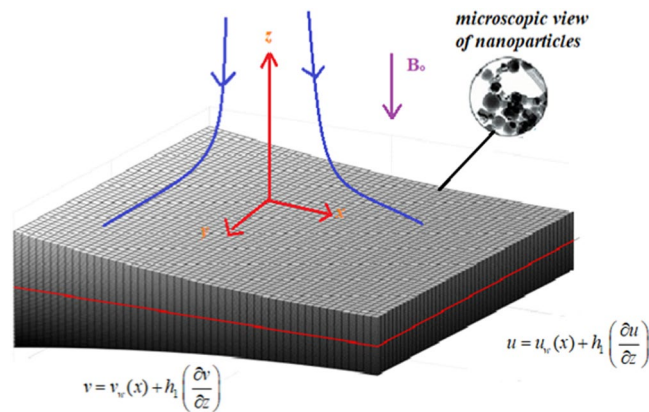


Figure 1. Schematic Model.

Benos *et al.*¹⁶. They noticed that variation in the shape of the nanomaterials tends to enhance heat transfer performance. Moreover, Chamkha¹⁷ discussed numerically the impression of magnetic properties over the nano liquid flow caused due cylinder in a three-dimensional enclosure by the aid of the finite element method. Meanwhile, the joint response of Prandtl number and magnetic properties over the 2D steady motion of nanofluid past a stretched membrane was numerically explored by Ganesh *et al.*¹⁸. As per the available literature, several researchers (19–23) did the outstanding work on applying MHD concept in their analysis.

Radiative thermal emission found vital applications in industrial engineering as the construction of gas turbines, design of fin and missiles, etc. Khan *et al.*²⁴ deliberated the 2-D flow of nano liquid through melting plane under the response of radiative heat flux²⁴. They revealed that hike in thermal radiation results in the improvement of heat transfer performance of the liquid. Seth *et al.*²⁵ examined semi analytically with the aid of OHAM to study the flow of nanofluid through an elongated plane by the implication of magnetic properties and also examined the entropy generation. Further, the researchers^{26–31} made noticeable results their analysis in convective heat transfer. Acharya *et al.*³² explored a computational work for analyzing the multiple slip effects on chemically reacting Williamson fluid flow in permeable medium. A hybrid approach for investigating the thermal radiation and hall current effects on nanofluid flow over a spinning disk was proposed by Acharya *et al.*³³. The effect of aligned magnetic field on the slippery flow of nanofluid was numerically studied by Acharya *et al.*³⁴. The researchers^{35,36} investigated the convective heat transport in different nanofluids using NDM and Lie group approaches. Effect of internal heat source and radiation on 3-D flow of nanofluid past a shrinking sheet was theoretically studied by Sharma *et al.*³⁷. The researchers^{38,39} investigated the natural convection in magnetohydrodynamic flow under various physical effects. Thermal radiation effect on magnetohydrodynamic flow in the presence of heat generation was numerically studied by the researchers^{40,41}. Boling *et al.*⁴² proposed a stability solution for the MHD equation. The researchers^{43,44} studied the magnetohydrodynamic flow of Power-Law fluid by considering the various flow geometries. Recently, Tlili *et al.*^{45,46} premeditated the magnetohydrodynamic flow of nanofluid by considering the various physical effects and flow geometries.

Recent days, variety of nanomaterial are discovered in literature, among these aluminum alloy nanoparticles AA7075 and AA7072 are of special featured nanomaterial with greater thermal, chemical and physical properties. Aluminum alloy plays a prominent role in aerospace industries, especially, aluminum alloys AA7072 and AA7075 are of abundant significance in the production of transport appliances namely, glider aircraft, rocket climbing frame, etc.²⁹. It is evident that very less work has found in the study of hybrid nanofluids. This article reports the 3-D magnetohydrodynamic flow of hybrid nanofluid across a stretched plane of non-uniform thickness with slip effects. We pondered aluminum alloys of AA7072 and AA7072 + AA7075 in methanol liquid. The numerical solutions are attained, and the role of physical factors on the flow phenomenon is analyzed and reflected by plots and numerical interpretations.

Formulation

3D MHD, steady flow of hybrid nanofluid past a stretched plane of non-uniform thickness with slip effect is considered. The hybrid nanofluid is composed of alloy nanoparticles of AA7072 and AA7072 + AA7075 suspended in methanol liquid.

The sheet of non-uniform thickness is considered as $z = A\delta^{(1-n)/2}$, $\delta = x + y + c$, $n \neq 1$ we have chosen A is small. It is also presumed, the sheet temperature as $T_w = T_0\delta^{\frac{1-n}{2}} + T_\infty$. The induced magnetic field is ignored in this study. Here B_0 is the magnetic field applied in parallel with the z -axis as revealed in Fig. 1. With conventions made above, the governing equations in vector form can be expressed as³⁰:

$$\nabla \cdot q = 0, \quad (1)$$

$$\rho_{hmf}(q \cdot (\nabla u)) = \mu_{hmf} \nabla^2 u - \sigma_{hmf} B^2 u, \quad (2)$$

$$\rho_{hnf}(q \cdot (\nabla v)) = \mu_{hnf} \nabla^2 v - \sigma_{hnf} B^2 v, \tag{3}$$

$$(\rho c_p)_{hnf}(q \cdot (\nabla T)) = k_{hnf} \nabla^2 T, \tag{4}$$

the linked boundary restrictions are

$$\left. \begin{aligned} u - u_w(x) - h_1 \left(\frac{\partial u}{\partial z} \right) &= 0, \quad v - v_w(x) - h_1 \left(\frac{\partial v}{\partial z} \right) = 0, \\ T - T_w(x) - h_2 \left(\frac{\partial T}{\partial z} \right) &= 0, \\ \text{and } u, v &\rightarrow 0, \quad T \rightarrow T_\infty \text{ as } z \rightarrow \infty \end{aligned} \right\} \tag{5}$$

where

$$\left. \begin{aligned} \zeta_1 &= \frac{k_B T}{\sqrt{2} \pi d^2 p}, \quad \delta = x + y + c, \quad h_1 = \left[\frac{2 - f_1}{f_1} \right] \zeta_1 \delta^{\frac{1-n}{2}}, \\ \zeta_2 &= \left(\frac{2\gamma}{\gamma + 1} \right) \frac{\zeta_1}{\text{Pr}}, \quad h_2 = \left[\frac{2 - b}{b} \right] \zeta_2 \delta^{\frac{1-n}{2}}, \quad B = B_0 \delta^{0.5(n-1)}, \end{aligned} \right\} \tag{6}$$

$$u_w = a \delta^{(1/2)(n-1)}, \quad v_w = a \delta^n, \quad T_w - T_\infty = T_0 \delta^{\frac{1-n}{2}}, \quad \text{for } n \neq 1, \tag{7}$$

The hybrid nanofluid parameters ρ_{hnf} , μ_{hnf} , σ_{hnf} , k_{hnf} represent the density, dynamic viscosity, electrical conductivity, thermal conductivity can be used as²⁶:

$$\left. \begin{aligned} \frac{k_{hnf}}{k_f} &= \frac{2(1 - \phi)k_f + (1 + 2\phi_{1s})k_{1s} + (1 + 2\phi_{2s})k_{2s}}{(2 + \phi)k_f + (1 - \phi_1)k_{1s} + (1 - \phi_2)k_{2s}}, \\ \frac{\rho_{hnf}}{\rho_f} &= (1 - \phi) + \frac{\phi_{1s}\rho_{1s}}{\rho_f} + \frac{\phi_{2s}\rho_{2s}}{\rho_f}, \quad \frac{(\rho c_p)_{hnf}}{(\rho c_p)_f} = (1 - \phi) + \frac{\phi_{1s}(\rho c_p)_{1s} + \phi_{2s}(\rho c_p)_{2s}}{(\rho c_p)_f}, \\ \frac{\mu_{hnf}}{\mu_f} &= (1 - \phi)^{-2.5}, \quad \frac{\sigma_{hnf}}{\sigma_f} = \left[1 + \frac{3\sigma_{1s}\phi_{1s} + \phi_{2s}\sigma_{2s} - 3\phi\sigma_f}{\sigma_{1s}(1 - \phi_{1s}) + \sigma_{2s}(1 - \phi_{2s}) + (2 + \phi)\sigma_f} \right], \quad \phi = \phi_{1s} + \phi_{2s}, \end{aligned} \right\} \tag{8}$$

following similarity transformations are used for non-dimensionalisation

$$\left. \begin{aligned} \eta &= z \left(\frac{(n + 1)a}{2\nu} \right)^{1/2} \delta^{(n-1)/2}, \quad T - T_\infty - (T_w(x) - T_\infty)\theta = 0, \\ u - a\delta^n f'(\eta) &= 0, \quad v - a\delta^n g'(\eta) = 0, \\ w &= - \left(\frac{2a\nu}{n + 1} \right)^{0.5} \delta^{(n-1)0.5} \left[\frac{n + 1}{2}(f + g) + \eta \left(\frac{n - 1}{2} \right) (f' + g') \right] \end{aligned} \right\} \tag{9}$$

by making use of Eqs. (6-9), the Eqs. (1-5) can be transmuted as

$$\left. \begin{aligned} \frac{n + 1}{2(1 - \phi)^{2.5}} f''' - \left((1 - \phi) + \frac{\phi_{1s}\rho_{1s} + \phi_{2s}\rho_{2s}}{\rho_f} \right) \left(n(f')^2 + nf'g' - \frac{n + 1}{2}(f + g)f'' \right) \\ - \left(1 + \frac{3\sigma_{1s}\phi_{1s} + \phi_{2s}\sigma_{2s} - 3\phi\sigma_f}{\sigma_{1s}(1 - \phi_{1s}) + \sigma_{2s}(1 - \phi_{2s}) + (2 + \phi)\sigma_f} \right) Mf' &= 0, \end{aligned} \right\} \tag{10}$$

$$\left. \begin{aligned} \frac{n + 1}{2(1 - \phi)^{2.5}} g''' - \left((1 - \phi) + \frac{\phi_{1s}\rho_{1s} + \phi_{2s}\rho_{2s}}{\rho_f} \right) \left(n(g')^2 + nf'g' - \frac{n + 1}{2}(f + g)g'' \right) \\ - \left(1 + \frac{3\sigma_{1s}\phi_{1s} + \phi_{2s}\sigma_{2s} - 3\phi\sigma_f}{\sigma_{1s}(1 - \phi_{1s}) + \sigma_{2s}(1 - \phi_{2s}) + (2 + \phi)\sigma_f} \right) Mg' &= 0, \end{aligned} \right\} \tag{11}$$

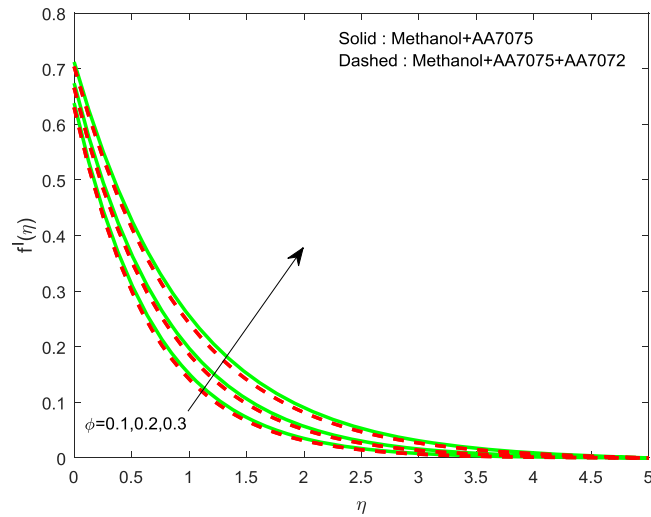


Figure 2. Impression of ϕ on $f'(\eta)$.

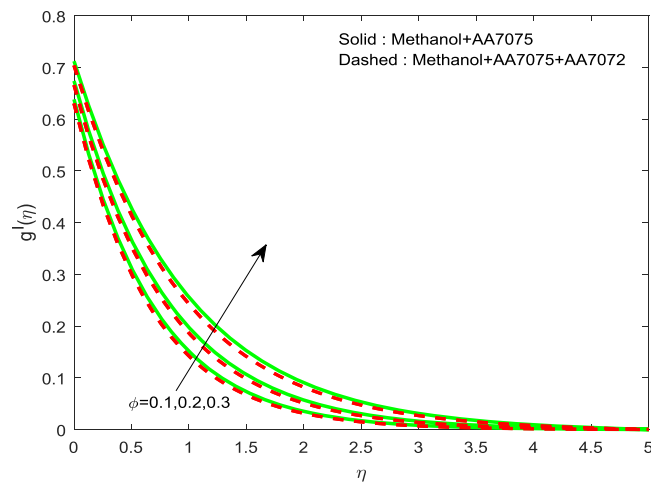


Figure 3. Impression of ϕ on $g'(\eta)$.

$$\left. \begin{aligned} & \left(\frac{2(1-\phi)k_f + (1+2\phi_{1s})k_{1s} + (1+2\phi_{2s})k_{2s}}{(2+\phi)k_f + (1-\phi_1)k_{1s} + (1-\phi_2)k_{2s}} \right) \theta'' \\ & - \frac{2Pr}{n+1} \left((1-\phi) + \frac{\phi_{1s}(\rho c_p)_{1s} + \phi_{2s}(\rho c_p)_{2s}}{(\rho c_p)_f} \right) \\ & \left(\frac{1-n}{2} \theta(f'+g') - \frac{n+1}{2} \theta'(f+g) \right) = 0, \end{aligned} \right\} \quad (12)$$

the transmuted boundary restrictions are

$$\left. \begin{aligned} f(0) &= \Lambda \left(\frac{1-n}{n+1} \right) [1 + h_1 f''(\eta)_{\eta=0}], f'(0) = [1 + h_1 f''(\eta)_{\eta=0}], \\ g(0) &= \Lambda \left(\frac{1-n}{n+1} \right) [1 + h_1 g''(\eta)_{\eta=0}], \theta(0) = [1 + h_2 \theta'(0)], \\ g'(0) &= [1 + h_1 g''(0)], f'(\eta)_{\eta \rightarrow \infty} = 0, g'(\eta)_{\eta \rightarrow \infty} = 0, \theta(\eta)_{\eta \rightarrow \infty} = 0, \end{aligned} \right\} \quad (13)$$

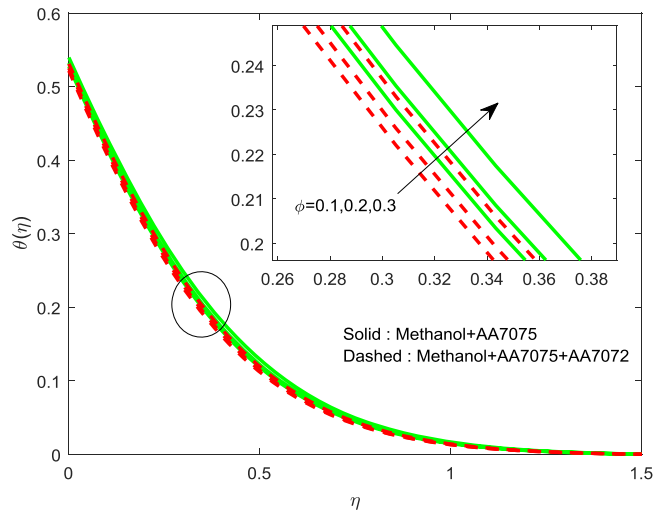


Figure 4. Impression of ϕ on $\theta(\eta)$.

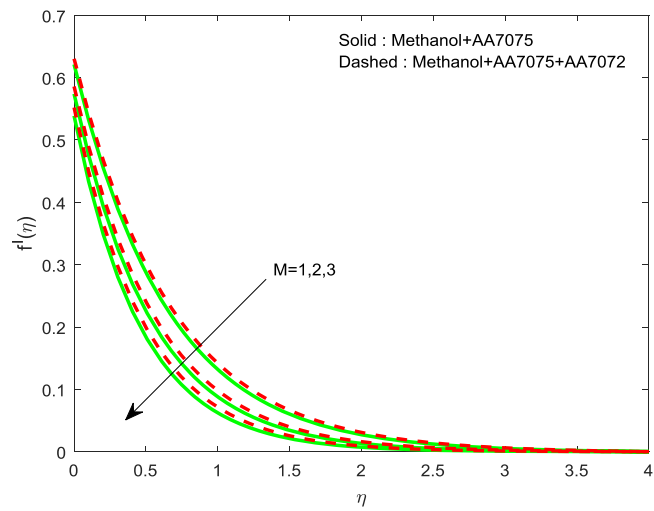


Figure 5. Impression of M on $f'(\eta)$.

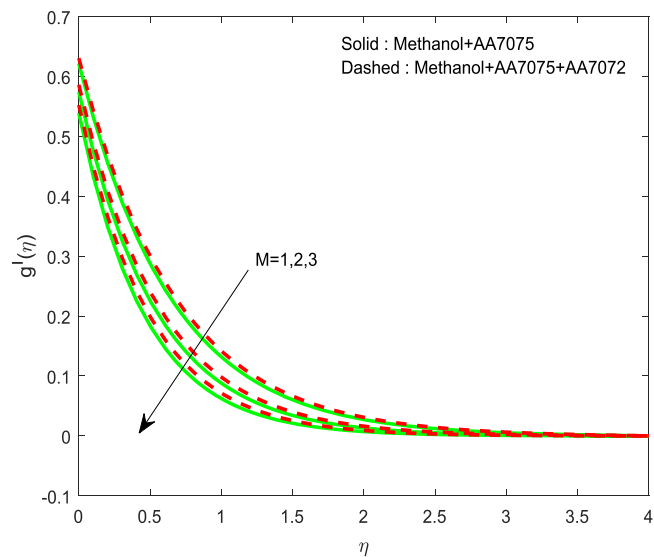


Figure 6. Impression of M on $g'(\eta)$.

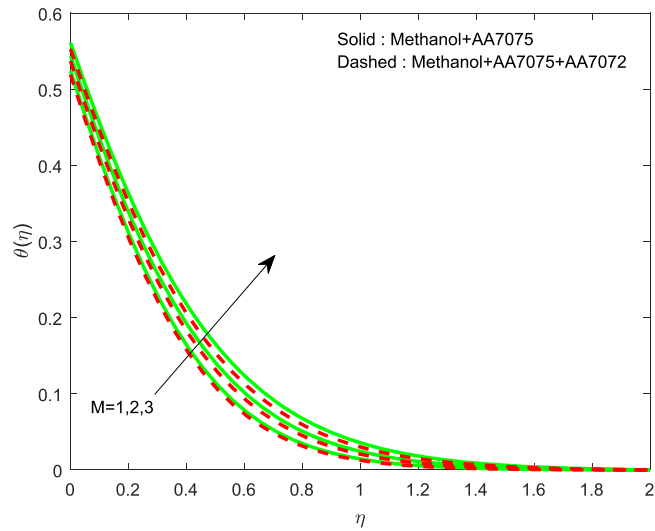


Figure 7. Impression of M on $\theta(\eta)$.

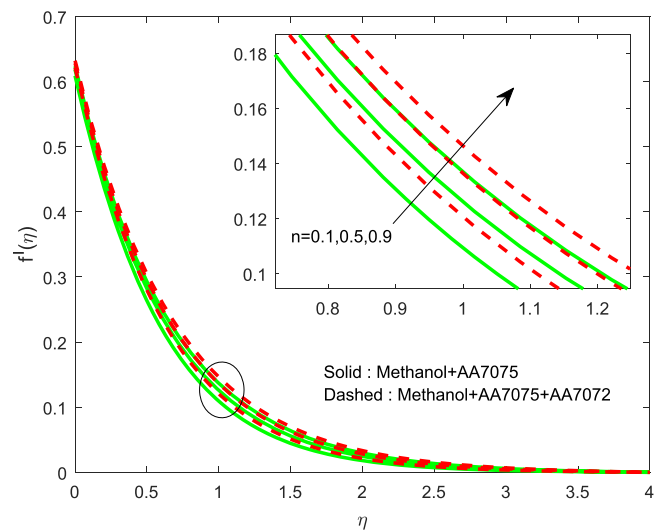


Figure 8. Impression of n on $f'(\eta)$.

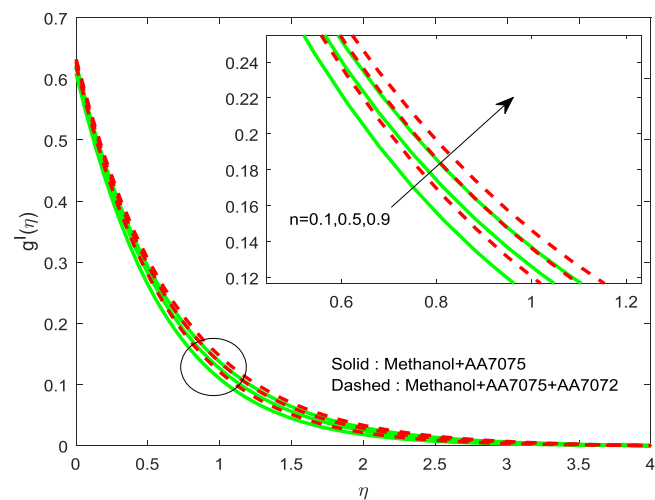


Figure 9. Impression of n on $g'(\eta)$.

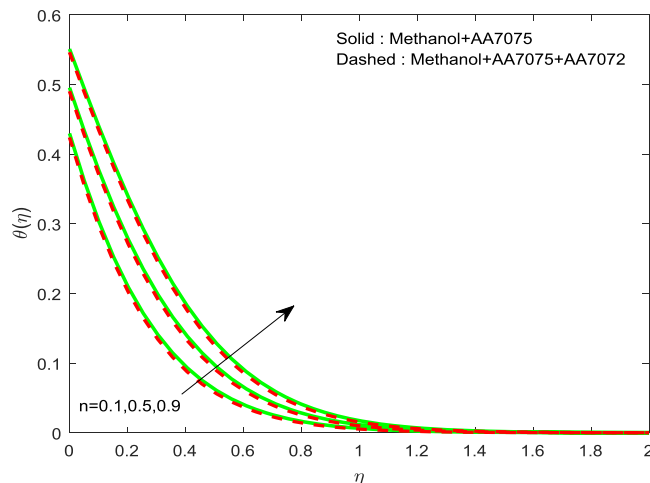


Figure 10. Impression of n on $\theta(\eta)$.

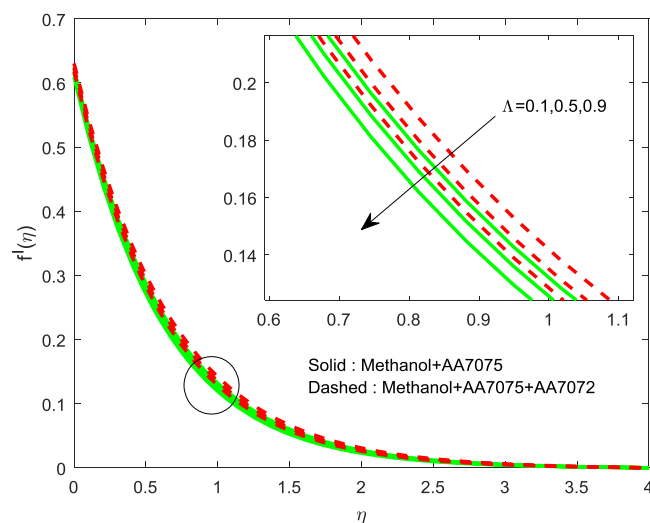


Figure 11. Impression of Λ on $f'(\eta)$.

where

$$M = \frac{\sigma_f B_0^2}{\rho_f a}, \text{Pr} = \frac{\mu_f (c_p)_f}{k_f}, \Lambda = \frac{1}{(1 - \phi)^{2.5}} \sqrt{\frac{(n + 1)a}{2\nu}}, \tag{14}$$

are the magnetic field parameter, Prandtl number and wall thickness parameters respectively. For engineering curiosity the C_f and Nu_x are defined as

$$C_f = 2 \frac{\mu_{hmf}}{\mu_f \sqrt{\text{Re}}} \left(\frac{n + 1}{2} \right)^{0.5} f''|_{\eta=0}, \quad Nu_x = - \sqrt{\text{Re}} \frac{k_{hmf}}{k_f} \left(\frac{n + 1}{2} \right)^{0.5} \theta'|_{\eta=0} \tag{15}$$

where $\text{Re} = \frac{u_w \delta}{\nu_f}$,

Results and Discussion

The system of ODE's (10–12) along the boundary restrictions (13) are resolved numerically using R-K based shooting procedure¹⁴. Impression of diverse dimensionless factors, volume fraction (ϕ), magnetic field (M), velocity power index (n), velocity slip (h_1), temperature jump (h_2), and wall thickness (Λ) over common profiles are revealed with plots and the influence of same restrictions on $f''(0)$ and $-\theta'(0)$ are depicted in a tabular manner. The physical parametric values are set to $M = 1$, $n = 0.7$, $h_1 = 0.4$, $h_2 = 0.4$, $\Lambda = 0.1$, $\text{Pr} = 7.38$ in order

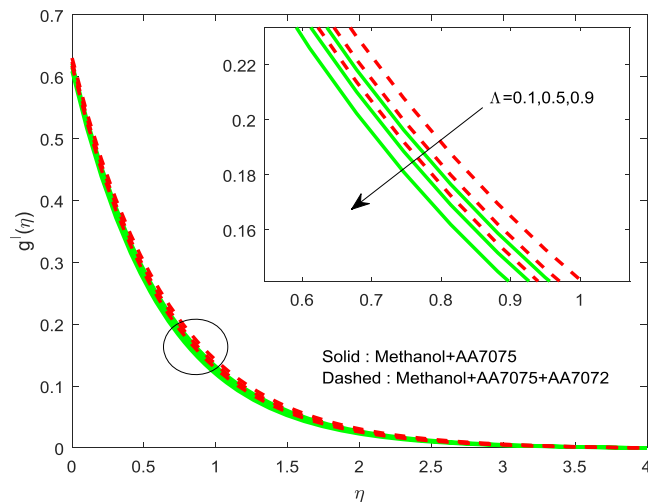


Figure 12. Impression of Λ on $g'(\eta)$.

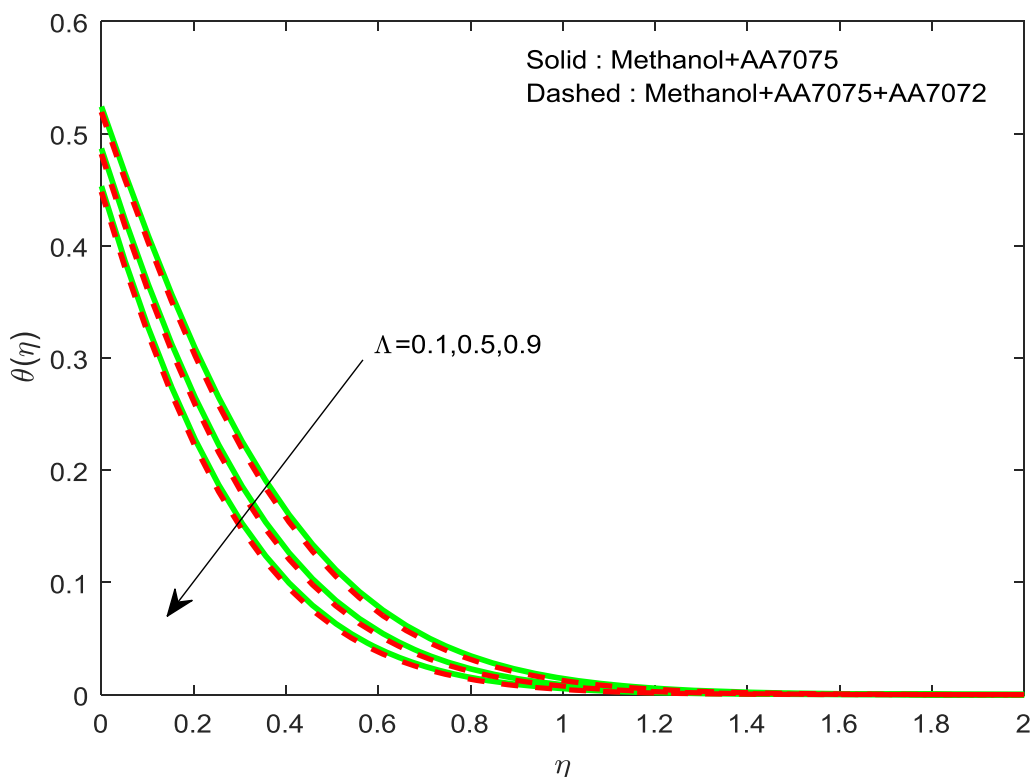


Figure 13. Impression of Λ on $\theta(\eta)$.

to attain the required results. Above quantities are reserved for the complete study, unless they specified in respective graphs and tables. Symbols used in figures $f'(\eta)$, $g'(\eta)$ and $\theta(\eta)$ describes the flow common quantities as velocity and temperature respectively. Simultaneous solutions are noticed for Methanol+AA7075 nanofluid and Methanol+AA7075 + AA7072 nanofluid. We treat Methanol+AA7075 nanofluid as first solution and Methanol+AA7075 + AA7072 nanofluid as second solution.

Figures 2–4 exhibits the impact of (ϕ) on $f'(\eta)$, $g'(\eta)$ and $\theta(\eta)$ we detect a hike in $f'(\eta)$, $g'(\eta)$ and $\theta(\eta)$ for improvement in volume of (ϕ) . The methanol+AA7075 nanofluid flow is highly influenced for rise in (ϕ) than Methanol+AA7075 + AA7072 nanofluid. Physically, rising the nanoparticle volume fraction leads to enhance the thermal conductivity of the fluid.

Figures 5–7 depicted to witness the effect of Lorentz force on $f'(\eta)$, $g'(\eta)$ and $\theta(\eta)$. We conclude that, increase in M upshots the reduction of $f'(\eta)$ and $g'(\eta)$. And a reverse trend is detected for $\theta(\eta)$. Physically, improvement in M leads to develop Lorentz force which in turn causes to resist the fluid motion, hence, we notice upswing in

Thermo Physical Properties	Methanol	AA7075	AA7072
$\rho(\text{Kg/m}^3)$	792	2810	2720
$c_p(\text{JKg}^{-1}\text{K}^{-1})$	2545	960	893
$k(\text{Wm}^{-1}\text{K}^{-1})$	0.2035	173	222
$\sigma(\text{S/m})$	0.5×10^{-6}	26.77×10^6	34.83×10^6

Table 1. Physio-thermal properties²⁹.

	ϕ	M	n	Λ	h_1	h_2	$f''(0)$	$-\theta'(0)$
Methanol+AA7075	0.1						-0.904541	1.189994
	0.2						-0.815286	1.183189
	0.3						-0.719774	1.171804
Methanol+AA7075 + AA7072	0.1						-0.924201	1.204535
	0.2						-0.835555	1.200096
	0.3						-0.740353	1.191678
Methanol+AA7075		1					-0.946854	1.191963
		2					-1.064841	1.140875
		3					-1.153017	1.096588
Methanol+AA7075 + AA7072		1					-0.924250	1.204508
		2					-1.035379	1.158209
		3					-1.119866	1.117809
Methanol+AA7075			0.1				-0.977908	1.427021
			0.5				-0.954347	1.263593
			0.9				-0.940993	1.125571
Methanol+AA7075 + AA7072			0.1				-0.947767	1.441625
			0.5				-0.929845	1.276739
			0.9				-0.919909	1.137567
Methanol+AA7075				0.1			-0.946854	1.191963
				0.5			-0.962395	1.285095
				0.9			-0.977748	1.368908
Methanol+AA7075 + AA7072				0.1			-0.924250	1.204508
				0.5			-0.939929	1.297872
				0.9			-0.955430	1.381794
Methanol+AA7075					0.2		-1.214595	1.260707
					0.4		-0.947198	1.191768
					0.6		-0.781192	1.137189
Methanol+AA7075 + AA7072					0.2		-1.180789	1.270845
					0.4		-0.924716	1.204259
					0.6		-0.764753	1.151438
Methanol+AA7075						0.2	-0.951100	1.561062
						0.4	-0.951100	1.189641
						0.6	-0.951100	0.960994
Methanol+AA7075 + AA7072						0.2	-0.929448	1.582044
						0.4	-0.929448	1.201788
						0.6	-0.929448	0.968904

Table 2. Values of $f''(0)$ and $-\theta'(0)$ for diverse non-dimensional constraints.

h_1	Λ	ref. ³¹	Present Results
0	0.2	-0.924828	-0.924828342
0.2	0.25	-0.733395	-0.733395213
0.2	0.5	-0.759570	-0.759570103

Table 3. Validation of the results for $f''(0)$ (2D case-water with $\phi = 0$) for various values of Λ and h_1 .

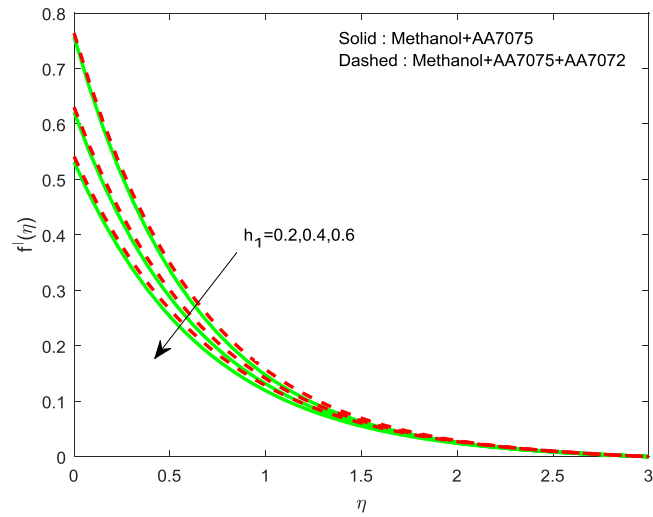


Figure 14. Impression of h_1 on $f'(\eta)$.

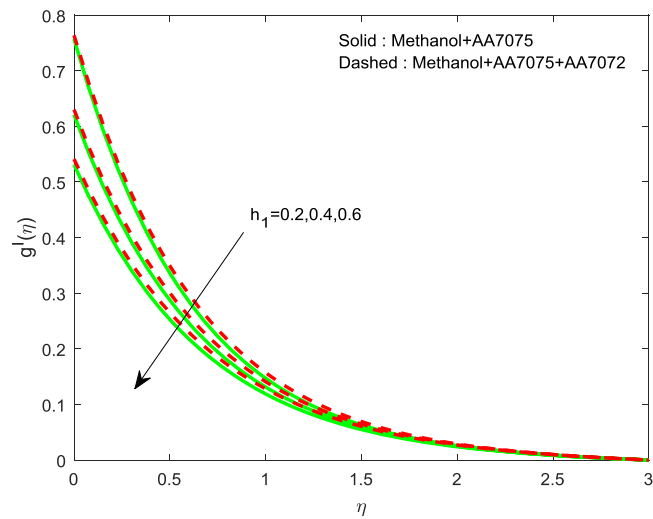


Figure 15. Impression of h_1 on $g'(\eta)$.

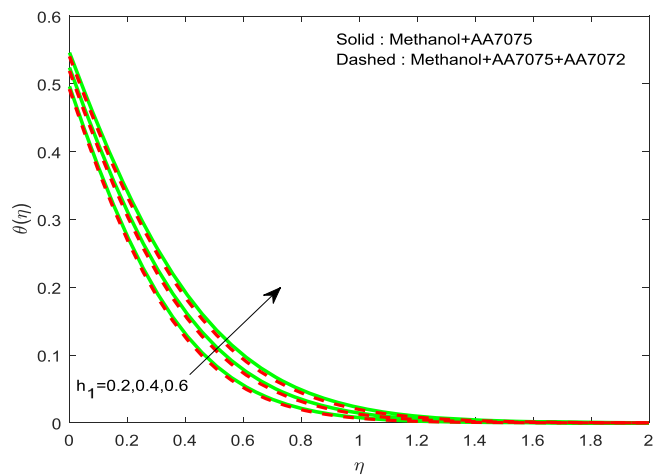


Figure 16. Impression of h_1 on $\theta(\eta)$.

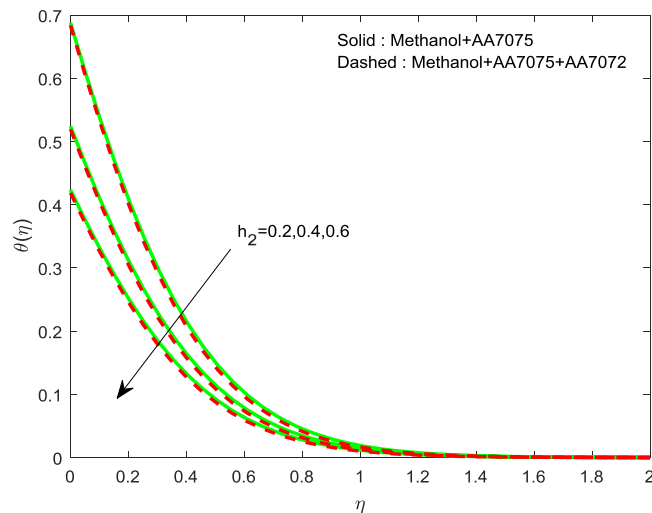


Figure 17. Impression of h_2 on $\theta(\eta)$.

thermal boundary layer. The existence of M diminishes the fluid motion of Methanol+AA7075 + AA7072 nanofluid over the Methanol+AA7075 nanofluid

Figures 8–10 are depicted to ascertain the nature of the curvatures $f'(\eta)$, $g'(\eta)$ and $\theta(\eta)$ under the influence of n . It is clear that, rise in n improves the distributions for $f'(\eta)$, $g'(\eta)$ and $\theta(\eta)$. Actually, boosting n helps in slendering of the sheet. It leads to, weaken the thickness of the sheet and in turn it enhances the thermal boundary layers. Figures 11–13 outlined to witness the consequences of Λ on $f'(\eta)$, $g'(\eta)$ and $\theta(\eta)$. We found that, $f'(\eta)$, $g'(\eta)$ and $\theta(\eta)$ are decreasing function of Λ . This concur the physical nature of the wall thickness parameter.

Figures 14–16 are portrayed to witness the changes in $f'(\eta)$, $g'(\eta)$ and $\theta(\eta)$ for diverse values of h_1 . It is evident that, escalating values of h_1 improves $\theta(\eta)$, but reverse nature is observed for $f'(\eta)$ and $g'(\eta)$. Finally, Fig. 17 exhibits the impact of h_2 on $\theta(\eta)$. It is obvious that, temperature distributions are diminishing functions of h_2 .

Table 1 portrays the basic properties of base liquid and nanoscaled materials. The disparity in skin friction factor $f''(0)$ and Nusselt number $-\theta'(0)$ under the influence of flow parameters ϕ , M , n , Λ , h_1 and h_2 are depicted in Table 2. The following observations are made, improved values of M and n results in declination of both skin friction coefficient and rate of heat transfer. It also worth noting that, the values $f''(0)$ and $-\theta'(0)$ of methanol+AA7072 + AA7075 nanofluid are more influenced by the varied values of M and n when compared with methanol+AA7075 nanofluid. Rate of heat transfer is a rising function of Λ , and $-\theta'(0)$ of methanol+AA7072 + AA7075 solution is high as equated with methanol+AA7075 solution. They are intensifying the values of ϕ and h_1 , both the parameters $f''(0)$ and $-\theta'(0)$ decelerates. Thermal transport rate of the nanofluids diminishes for improved vales of h_2 . The validation of the present results is depicted in Table 3.

Conclusions

A 3D MHD flow of hybrid nanofluid over a surface of non-uniform thickness with slip effects is studied numerically. We pondered aluminum alloys of AA7072 and AA7072 + AA7075 in methanol liquid and presented simultaneous solutions. The significant outcomes are as follows:

- Momentum and thermal distributions are increasing functions of n .
- Flow field is diminished by magnetic field parameter, M and a reverse trend is observed for the temperature field.
- The hike in wall thickness parameter results in a lessening in the flow and energy fields.
- The impact of Lorentz force is less on hybrid nanofluid when equated with nanofluid.
- The rate of thermal transport of the hybrid nanofluid is higher than the nanofluid.
- Wall thickness parameter regulates the Nusselt number for both the nanofluids.
- The major application of the present study can be found in aerospace manufacturing industries.

Received: 24 October 2019; Accepted: 19 February 2020;

Published online: 06 March 2020

References

1. Choi, S. U. S. & Eastman, J. A. Enhancing thermal conductivity of fluids with nanoparticles. *ASME-Pub-Feb* **231**, 99–106 (1995).
2. Acharya, N., Das, K. & Kumar, P., On the heat transport mechanism and entropy generation in a nozzle of liquid rocket engine using ferrofluid: A computational framework, *J. Comput. Des. Eng.* Article in press 1–12, <https://doi.org/10.1016/j.jcde.2019.02.003> (2019).
3. Şenay, G., Kaya, M., Gedik, E. & Kayfeci, M. Numerical investigation on turbulent convective heat transfer of nanofluid flow in a square cross-sectioned duct. *Int. J. Numer. Methods Heat Fluid Flow*. **29**, 1432–1447 (2019).

4. Saleem, S. *et al.* Heat transfer in a permeable cavity filled with a ferrofluid under electric force and radiation effects Heat transfer in a permeable cavity filled with a ferrofluid under electric force and radiation effects. *AIP Adv.* **9**, 1–9 (2019).
5. Hosseinzadeh, K., Afsharpanah, F., Zamani, S., Gholinia, M. & Ganji, D. D. A numerical investigation on ethylene glycol-titanium dioxide nano fluid convective flow over a stretching sheet in presence of heat generation/absorption, *Case Stud. Therm. Eng.* **12**, 228–236 (2018).
6. Wang, L., Huang, C., Yang, X., Chai, Z. & Shi, B. Effects of temperature-dependent properties on natural convection of power-law nanofluids in rectangular cavities with sinusoidal temperature distribution. *Int. J. Heat Mass Transf.* **128**, 688–699 (2019).
7. Waqas, M., Khan, M. I., Hayat, T., Gulzar, M. M. & Alsaedi, A. Transportation of radiative energy in viscoelastic nanofluid considering buoyancy forces and convective conditions, Chaos, Solitons Fractals Interdiscip. *J. Nonlinear Sci. Nonequilibrium Complex Phenom.* **130**, 1–7 (2020).
8. Ajeel, R. K., Salim, W. S. W. & Hasnan, K. Thermal performance comparison of various corrugated channels using nanofluid: Numerical study. *Alexandria Eng. J.* **58**, 75–87 (2019).
9. Al-Rashed, A. A. A. Investigating the effect of alumina nanoparticles on heat transfer and entropy generation inside a square enclosure equipped with two inclined blades under magnetic field. *Int. J. Mech. Sci.* **152**, 312–328 (2019).
10. Ahmad, B., Iqbal, Z., Maraj, E. N. & Ijaz, S. Utilization of elastic deformation on Cu-Ag nanoscale particles mixed in hydrogen oxide with unique features of heat generation/absorption: closed form outcomes. *Arab. J. Sci. Eng.* **44**, 5949–5960 (2019).
11. Akbarzadeh, P. & Mahian, O. The onset of nanofluid natural convection inside a porous layer with rough boundaries. *J. Mol. Liq.* **272**, 344–352 (2018).
12. Animasaun, I. L. *et al.* Comparative analysis between 36 nm and 47 nm alumina-water nanofluid flows in the presence of Hall effect. *J. Therm. Anal. Calorim.* **135**, 873–886 (2019).
13. Asadi, A., Nezhad, A. H., Sarhaddi, F. & Keykha, T. Laminar ferrofluid heat transfer in presence of non-uniform magnetic field in a channel with sinusoidal wall: a numerical study. *J. Magn. Magn. Mater.* **471**, 56–63 (2018).
14. Kumar, K. A., Sugunamma, V., Sandeep, N. & Reddy, J. V. R. MHD stagnation point flow of Williamson and Casson fluids past an extended cylinder: a new heat flux model, *Appl. Sci.* **1**, 1–11 (2019).
15. Bai, Y., Xie, B., Zhang, Y., Cao, Y. & Shen, Y. Stagnation-point flow and heat transfer of upper-convected Oldroyd-B MHD nano fluid with Cattaneo-Christov double-diffusion model. *Int. J. Numer. Methods Heat Fluid Flow.* **29**, 1039–1057 (2018).
16. Benos, L. T., Karvelas, E. G. & Sarris, I. E. A theoretical model for the magnetohydrodynamic natural convection of a CNT-water nanofluid incorporating a renovated Hamilton-Crosser model. *Int. J. Heat Mass Transf.* **135**, 548–560 (2019).
17. Chamkha, A. J. & Selimefendigil, F., MHD mixed convection of nanofluid due to an inner rotating cylinder in a 3D enclosure with a phase change material. *Int. J. Numer. Methods Heat Fluid Flow.* Article in press, <https://doi.org/10.1108/HFF-07-2018-0364> (2018).
18. Ganesh, N. V., Al-mdallal, Q. M. & Kameswaran, P. K. Numerical study of MHD effective Prandtl number boundary layer flow of γ Al_2O_3 nanofluids past a melting surface. *Case Stud. Therm. Eng.* **13**, 100413, <https://doi.org/10.1016/j.csite.2019.100413> (2019).
19. Ramudu, A. C. V., Kumar, K. A., Sugunamma, V. & Sandeep, N. Influence of suction/injection on MHD Casson fluid flow over a vertical stretching surface. *J. Therm. Anal. Calorim.* **7**, 1–8 (2019).
20. Li, Z., Shafee, A., Ramzan, M., Rokni, H. B. & Al-mdallal, Q. M. Simulation of natural convection of Fe_3O_4 -water ferrofluid in a circular porous cavity in the presence of a magnetic field. *Eur. Phys. J. Plus.* **134**, 1–8 (2019).
21. Samrat, S. P., Sulochana, C. & Ashwinkumar, G. P. Impact of thermal radiation on an unsteady Casson nanofluid flow over a stretching surface. *Int. J. Appl. Comput. Math.* **5**, 1–20 (2019).
22. Tlili, I., Khan, W. A. & Ramadan, K. MHD Flow of Nanofluid Flow Across Horizontal Circular Cylinder: Steady Forced Convection. *Journal of Nanofluids* **8**, 179–186 (2019).
23. Tlili, I., Khan, W. A. & Khan, I. Multiple slips effects on MHD SA- Al_2O_3 and SA-Cu non-Newtonian nanofluids flow over a stretching cylinder in porous medium with radiation and chemical reaction. *Results in Physics.* **8**, 213–222 (2019).
24. Khan, M. I., Hayat, T., Waqas, M., Alsaedi, A. & Khan, M. I. Effectiveness of radiative heat flux in MHD flow of Jeffrey-nanofluid subject to Brownian and thermophoresis diffusions. *J. Hydrodyn.* **31**, 421–427 (2019).
25. Seth, G. S., Bhattacharyya, A., Kumar, R. & Chamkha, A. J. Entropy generation in hydromagnetic nanofluid flow over a non-linear stretching sheet with Navier's velocity slip and convective heat transfer. *Phys. Fluids.* **30**, 122003, <https://doi.org/10.1063/1.5054099> (2018).
26. Dinarvand, S. Nodal/saddle stagnation-point boundary layer flow of CuO-Ag/water hybrid nanofluid: a novel hybridity mode. *Microsystem Technologies* **25**(7), 2609–2623 (2019).
27. Sheikholeslami, M., Khan, I. & Tlili, I., Non-equilibrium Model for Nanofluid Free Convection Inside a Porous Cavity Considering Lorentz Forces, *Scientific Reports* **8**, Article number: 16881 (2018)
28. Ghadikolaei, S. S., Hosseinzadeh, K. & Ganji, D. D. Investigation on ethylene glycol-water mixture fluid suspended by hybrid nanoparticles (TiO_2 -CuO) over rotating cone with considering nanoparticles shape factor. *J. Mol. Liq.* **272**, 226–236 (2018).
29. Sandeep, N. & Animasaun, I. L. Heat transfer in wall jet flow of magnetic-nanofluids with variable magnetic field. *Alexandria Eng. J.* **56**, 263–269 (2017).
30. Babu, M. J. & Sandeep, N. 3D MHD slip flow of a nanofluid over a slendering stretching sheet with thermophoresis and Brownian motion effects. *Journal of Molecular Liquids* **222**, 1003–1009 (2016).
31. Khader, M. & Megahed, A. M. Numerical solution for boundary layer flow due to a nonlinearly stretching sheet with variable thickness and slip velocity. *The European Physical Journal Plus* **128**(9), 1–7 (2013).
32. Acharya, N., Das, K. & Kundu, P. K. Influence of multiple slips and chemical reaction on radiative MHD Williamson nanofluid flow in porous medium: A computational framework, Multidiscipline Modeling in. *Materials and Structures* **15**(3), 630–658 (2019).
33. Acharya, N., Raju, B. & Kundu, P. K. Influence of Hall current on radiative nanofluid flow over a spinning disk: A hybrid approach. *Physica E: Low-dimensional Systems and Nanostructures* **111**, 103–112 (2019).
34. Acharya, N., Maity, S. & Kundu, P. K., Influence of inclined magnetic field on the flow of condensed nanomaterial over a slippery surface: the hybrid visualization, *Appl. Nanosci.* <https://doi.org/10.1007/s13204-019-01123-0> (2019).
35. Acharya, N., Das, K. & Kundu, P. K. Ramification of variable thickness on MHD TiO_2 and Ag nanofluid flow over a slendering stretching sheet using NDM. *EPJ Plus* **131**, ID:303 (2016).
36. Das, K., Acharya, N. & Kundu, P. K. The onset of nanofluid flow past a convectively heated shrinking sheet in presence of heat source/sink: A Lie group approach. *Applied Thermal Engineering* **103**, 38–46 (2016).
37. Sharma, R. P., Seshadri, R., Mishra, S. R. & Munjam, S. R. Effect of thermal radiation on MHD three-dimensional motion of nanofluid past a shrinking surface under the influence of heat source, *Heat Transfer - Asian. Research* **48**(6), 2105–2121 (2019).
38. Sharma, R. P. & Paul, A. Transient natural convection magnetohydrodynamic motion over an exponentially accelerated vertical porous plate with heat source. *Indian Journal of Pure & Applied Physics* **57**, 205–211 (2019).
39. Saranya, S., Ragupathi, P., Ganga, B., Sharma, R. P. & Abdul Hakeem, A. K. Non-linear radiation effects on magnetic/non-magnetic nanoparticles with different base fluids over a flat plate. *Advanced Powder Technology* **29**, 1977–1990 (2018).
40. Gaur, P. K., Sharma, R. P. & Jha, A. K. Transient free convective radiative flow between vertical parallel plates heated/cooled asymmetrically with heat generation and slip condition. *International Journal of Applied Mechanics and Engineering* **23**(2), 365–384 (2018).
41. Sharma, R. P., Murthy, P. V. S. N. & Devendra, K. Transient free convection MHD flow of a nanofluid past a vertical plate with radiation in the presence of heat generation. *Journal of Nanofluids* **6**(1), 80–86 (2017).

42. Boling, G., Linghai, Z. & Haiyang, H. Long-time uniform stability of solution to magnetohydrodynamics equation. *Applied Mathematics-A Journal of Chinese Universities* **14**, ID.45 (1999).
43. Ellahi, R., Sait, S. M., Shehzad, N. & Mobin, N. Numerical Simulation and Mathematical Modeling of Electro-Osmotic Couette–Poiseuille Flow of MHD Power-Law Nanofluid with Entropy Generation. *Symmetry* **11**(8), 1038 (2019).
44. Shehzad, N., Zeeshan, A. & Ellahi, R. Electroosmotic Flow of MHD Power Law Al₂O₃-PVC Nanofluid in a Horizontal Channel: Couette–Poiseuille Flow Model. *Communications in Theoretical Physics* **69**, ID.655 (2017).
45. Tlili, I., Khan, W. A. & Ramadan, K. MHD flow of nanofluid flow across horizontal circular cylinder: steady forced convection. *J. Nanofluids*. **8**(1), 179–186 (2019).
46. Tlili, I., Khan, W. A. & Ramadan, K. Entropy generation due to MHD stagnation point flow of a nanofluid on a stretching surface in the presence of radiation. *J. Nanofluids*. **7**(5), 879–890 (2018).

Acknowledgements

Authors acknowledge the UGC, India for startup grant No. 30-489/2019(BSR).

Author contributions

I.T. & H.A.N. did the literature survey; G.P.A. discussed the results, N.S. formulated the problem. All authors look over the final script and approved.

Competing interests

The authors declare no competing interests.

Additional information

Correspondence and requests for materials should be addressed to G.P.A. or N.S.

Reprints and permissions information is available at www.nature.com/reprints.

Publisher's note Springer Nature remains neutral with regard to jurisdictional claims in published maps and institutional affiliations.



Open Access This article is licensed under a Creative Commons Attribution 4.0 International License, which permits use, sharing, adaptation, distribution and reproduction in any medium or format, as long as you give appropriate credit to the original author(s) and the source, provide a link to the Creative Commons license, and indicate if changes were made. The images or other third party material in this article are included in the article's Creative Commons license, unless indicated otherwise in a credit line to the material. If material is not included in the article's Creative Commons license and your intended use is not permitted by statutory regulation or exceeds the permitted use, you will need to obtain permission directly from the copyright holder. To view a copy of this license, visit <http://creativecommons.org/licenses/by/4.0/>.

© The Author(s) 2020